Pergamon

Calphad, Vol. 26, No. 1, pp. 95–118, 2002

0364-5916/02/$ - see front matter

PII: S0364-5916(02)00027-5

Thermodynamic Modeling of the Zr-O System

Raymundo Arroyave, Larry Kaufman , and Thomas W. Eagar

Department of Materials Science and Engineering,Room 4-134
Massachusetts Institute of Technology, Cambridge, MA 02139 USA
raymundo@mit.edu,larrykaufman@rcn.com,tweagar@mit.edu

(Received November 29, 2001)

Abstract. In this study, the complete zirconium-oxygen system has been critically assessed at 1 $at.$ from $300°C$ to liquidus temperatures. Thermochemical measurements and phase diagram data were used to model the Gibbs free energies of seven phases. Additionally, the ordered interstitial HCP-based solutions were included and considered as simple line compounds. By using the PARROT module in Thermo-Calc, it was possible to optimize the parameters of the models used to describe the Gibbs free energies of the HCP, BCC, $Liquid$, γ ZrO_{2-x},β ZrO_{2-x} and α ZrO_{2-x} phases. The Gas phase was considered to behave ideally. Although phase diagrams including the stoichiometric zirconia phases have been assessed, this is the first time, to the best of our knowledge that a complete assessment of this system is published. © 2002 Published by Elsevier Science Ltd.

1 Introduction

The Zr-O system has a wide range of technological applications. For example, since zirconium is an important component of low melting temperature, amorphous alloys(used in conjunction with nickel, titanium, aluminum), knowledge of the thermodynamics of the interactions between this element and oxygen would be helpful for assessing the oxidation behavior of such systems. In other cases, zirconia-based ceramics are often the materials of choice in high-temperature, engine components [1], due to their low thermal conductivity, high thermal expansion coefficients and higher fracture toughness as compared to most ceramic materials. This application involves the creation of ceramic/metal interfaces and it is expected that both during fabrication and normal operation, complex interfacial reactions may occur. It would be desirable to predict what kind of reaction products are likely to precipitate under certain thermal and chemical conditions as these products would determine the life span of the composite part.Another application where knowledge of the thermodynamics of zirconia-based ceramics becomes important is solid state oxide fuel cells. Complex reactions between electrodes (based on perovskite systems) and electrolytes (zirconia-based) tend to diminish the transport efficiency and life span of the fuel cells [2]. Predicting the thermodynamic stability of the different interfacial reaction products would be essential for the development of reliable and efficient fuel cells.

Despite considerable experimental work done on the problems described above, little generalization and extrapolation can be done if the proper thermodynamic model for the systems at hand is not available. With an adequate thermodynamic model, on the other hand, these problems could be treated in a more systematic way and the development times for such technologies could be reduced. Ideally, with a complete thermodynamic model it would be possible to predict the stability of all the possible phases formed, given a set of thermal and chemical conditions. One essential step towards that direction is the development of a reliable database for the thermochemical interactions in the Zr-O system.

To the best of our knowledge, the only thermodynamic modelling for the *elemental Zr-O* binary has been

done by Kaufman and Clougherty [3][1]. In their work, they considered the *BCC*, *HCP*, *Liquid* and the tetragonal $\beta\ ZrO_{2-x}$ non-stoichiometric phase. Considerably more information regarding the thermochemistry and phase boundaries of this system has been obtained over the past decades. This thermodynamic data can be used to produce a fully consistent thermodynamic model, which in turn can be incorporated in more complex databases relevant to several different areas of materials processing and development.

In this work, several semi-empirical models for the stable phases will be used to describe their Gibbs free energies as a function of composition and temperature. In these models, several adjustable parameters can be used to obtain an algebraic expression for the Gibbs free energies as a function of both composition and temperature. By using the thermochemical and phase diagram data available, it is possible to optimize these parameters so that a self-consistent thermodynamic model for the whole system can be obtained. For this work, the *PARROT* [4] module in the *Thermo-Calc* [5] program was used to minimize the error between the experimental information and the values calculated using the semi-empirical description of the Gibbs free energies of each of the phases of the system.

The aim of this work is to present a self-consistent model for the *Zr-O* system, from pure zirconium to pure oxygen, including all the known condensed phases and the gas phase. The database obtained from this work is expected to be used in conjunction with other metal, and metal-oxygen databases; thus, special attention was given to compatibility issues. As will be seen, this priority influenced the way some phases were modelled. Despite some necessary simplifications, the main features of the phase diagram and the thermochemical behavior of the system were acceptably reproduced.

2 Experimental Information

For the thermodynamic modelling of the stable phases of the *Zr-O* system, two different types of data were used. The first set of data corresponds to temperature-composition information,i.e. data on the phase boundaries and invariant points. The second group corresponds to measurements of the thermochemical properties of the different phases of the system. These measurements include determinations of the enthalpy of solution, oxygen partial pressures, etc. In this section, the complete set of experimental information, as well as an assessment of the validity of the data is presented.

2.1 Phase Diagram Information

The most complete critical assessment of the phase diagram information (refer to Fig. 2) on this system corresponds to the work by Abriata et al [6]. The $Zr-O$ system is of medium complexity, having several condensed-mixture phases, stoichiometric compounds and ordered-interstitial solutions:

The *Liquid* phase has been observed to go from purely metallic to purely ionic character in a continuous manner. The most complete and accurate determination of the liquidus has been done by Ackerman et al. [7]. Several important invariant equilibrium reactions have been determined: the high-zirconium peritectic ($L + HCP \rightleftharpoons BCC$), congruent melting ($L \rightleftharpoons HCP$) and eutectic($L \rightleftharpoons HCP + \gamma\ ZrO_{2-x}$). It has also been observed that at the stoichiometric composition ZrO_2, the high temperature cubic phase ($\gamma\ ZrO_{2-x}$) melts congruently at 2710°C. The study by Ackerman et. al differs greatly at some points ($170°C$ being the maximum difference) from previous investigations [8], however, Abriata et al. [6] have established that since the purity of the starting Zr metal was superior in the investigation done by Ackerman et al., this information has the greatest credibility.

McQuillan [9] was able to determine that oxygen dissolves interstitially in $BCC-Ti$. It is then reasonable to assume that the same behavior would be present in $BCC-Zr$ solid solutions. This phase has a maximum oxygen solubility of 10.5 $at.\%$ at $1970°C$, which is the temperature of the peritectic reaction. The $BCC/(BCC+HCP)$

[1]This is quite surprising, given the importance that this system has on several technologies developed in the past few years

phase boundary was determined by metallography and electrical resistivity by two different groups [8], [10]. In general the phase boundaries agree well, although there is a slight variation in the compositions, specially at temperatures close to the peritectic point.

The HCP phase dissolves oxygen interstitially [11] and the maximum solubility of oxygen has been reported to be 35 $at.\%$ at the eutectic temperature ($2065°C$). It has been observed that at high temperatures ($> 400°C$) and low concentrations, oxygen occupies the larger interstitial sites (octahedral holes) randomly. As temperature decreases and/or the oxygen content increases, it has been observed that oxygen tends to partially order at temperatures below $900°C$ [12]. As temperature decreases, it has been observed that there are three possibly distinct fully ordered interstitial phases, centered around the $0.16, 0.25$ ***and*** 0.333 $at.\%$ oxygen concentrations [12], although this region of the phase diagram is rather speculative.

The (Zr-rich side) $HCP/(HCP + \gamma\ ZrO_{2-x})$ phase boundary has been investigated using electrical resistivity [10] and solid-solid diffusion [7] methods. In general there is very good agreement between both sets of data. The $HCP/(HCP + \beta\ ZrO_{2-x})$ phase boundary has been also investigated by the same groups and the agreement is quite good. The $HCP/(HCP + \alpha\ ZrO_{2-x})$ phase boundary was investigated using metallographic techniques [8] and shows that the solubility limit of oxygen in HCP is virtually independent of concentration, at low temperatures. The $(HCP + \beta\ ZrO_{2-x})/\beta\ ZrO_{2-x}$ phase boundary was investigated by [13] while the $(HCP + \gamma\ ZrO_{2-x})/\gamma\ ZrO_{2-x}$ phase boundary was investigated by [14] and [10]. The $(Liquid + \gamma\ ZrO_{2-x})/\gamma\ ZrO_{2-x}$ phase boundary was investigated by [7] and was shown to present retrograde solubility with a minimum oxygen content of $61at.\%$ at $2300°C$.

The compound ZrO_{2-x} has been observed to have varying degrees of stoichiometry (where $0 < x < 0.44$). The higher-temperature phase $\gamma\ ZrO_{2-x}$ has a cubic structure isomorphic with CaF_2 and shows a high degree of non-stoichiometry (measured using isopiestic equilibration), the non-stoichiometric region of the phase being stable at temperatures as low as $1525°C$ [15], [7], [14] which is much lower than the coherent transformation to the $\beta\ ZrO_{2-x}$ phase($\sim 2377°C$ [15]). The $\gamma\ ZrO_{2-x}$ phase exhibits a congruent melting point at $2710°C$. The $\beta\ ZrO_{2-x}$ phase (tetragonal) has a much narrower degree of non-stoichiometry and is isomorphic to HgI_2. At $1205°C$, this phase transforms to $\alpha\ ZrO_{2-x}$ [15]. The $(\gamma\ ZrO_{2-x} + \beta\ ZrO_{2-x})/\beta\ ZrO_{2-x}$ phase boundary has been studied using mass spectroscopy [13], and has been determined to lie at $x < 0.02$. It has also been observed [13] that there exists an invariant transformation $\gamma\ ZrO_{2-x} \rightleftharpoons HCP + \beta\ ZrO_{2-x}$ at $1525°C$. The low temperature $\alpha\ ZrO_{2-x}$ monoclinic phase has been observed to be nearly stoichiometric and there is no information regarding the maximum degree of non-stoichiometry that it presents. None of these phases have been observed to oxidize beyond stoichiometry. Therefore, a $ZrO_2 + O(g)$ two-phase field must exist at compositions above 66.6 $at.\%$. This will be observed in the calculated phase diagram obtained in this work.

2.2 Thermochemical Measurements

2.2.1 BCC and (BCC + HCP) Solid Solutions

Because of the difficulty to measure the extremely low oxygen pressures in equilibrium with *BCC* solid solutions, the only experimental data available for the *BCC* phase corresponds to the molar partial enthalpies of oxygen. Boureau and Gerdanian [16], for example, used micro-calorimetric techniques to determine the partial enthalpy of oxygen in $BCC(\Delta\overline{H}(O_2))$. In this technique, the heat released when small amounts of oxygen are blown over a small sample of *BCC-Zr* was measured and related to the oxygen partial enthalpy. For this method to work, the oxygen needs to reach all parts of the zirconium surface at the same time. This means that the sample must be rather small, increasing the difficulty to measure any heat effect. Therefore, the smaller the sample, the greater the expected error ($+/-5\%$ in [16]). From these experiments, it was determined that within this phase, the oxygen partial enthalpy is virtually independent of composition and with a reported value of $\Delta\overline{H}(O_2) = -1,194\frac{kJ}{mol}$ at $1050°C$.Boureau et al [16] measured the oxygen partial enthalpy at $1050°C$ in the $(BCC + HCP)$ phase field, obtaining a value of $\Delta\overline{H}(O_2) = -1287\frac{kJ}{mol}$ of O_2.

2.2.2 *HCP Solid Solutions*

The oxygen partial molar enthalpy in HCP solid solutions was measured in two different occasions using microcalorimetric techniques (See [17] and [16]). It was found that at low oxygen contents ($X(O) < 0.16$) the partial molar enthalpy was essentially constant ($\triangle\overline{H}(O_2) \sim -1,190\frac{kJ}{mol}$). However, when passing this range, the value for $\triangle\overline{H}(O_2)$ has been observed to drop sharply. This behavior has been correlated to the existence of ordered phases at lower temperatures in other transition metal-oxygen systems, such as *Ti-O* and *Hf-O* [16]. It will be observed that the model obtained in this work reproduces this behavior.

Komarek and Silver [18] determined the thermochemical properties (partial molar free energies, enthalpies and entropies) of HCP solid solutions between the ranges $800°C$ to $1000°C$ by reacting the thin metal samples at a given temperature with an excess of a mixture of an alkaline earth metal, *M*, and its oxide until equilibrium was reached, i.e. until the partial pressure of oxygen of the alloy was equal to the partial pressure of oxygen given by the reaction

$$M(l,s) + \frac{1}{2}O_2(g) \rightleftharpoons MO(s) \tag{1}$$

The standard free energy change $\triangle^0 G$, for this reaction is given by:

$$\triangle^0 G^1 = RT\ln(P_{O_2}^{1/2}) \tag{2}$$

The relative partial molar free energy of oxygen in the alloy (per g-atom oxygen) is given by:

$$\mu(O) = RT\ln(a_O) = RT\ln(P_{O_2}^{1/2}) \tag{3}$$

Using this method, the range of compositions that can be investigated is rather limited [18]. Therefore, an additional method was used to explore the high-oxygen content regions of the HCP phase field. In this method, the metal samples were placed inside the reactor in contact with the earth metal-oxide and were equilibrated with the earth metal vapor. The vapor pressure of the earth metal was kept constant by placing a source for the metal at a lower temperature inside the furnace. By controlling this low temperature, it was possible to modify the equilibrium conditions. The equations for the oxygen equilibrium were combined with the evaporation, sublimation reactions:

$$M(l,s) \rightleftharpoons M(g) \tag{4}$$

Combining Eqns. (1) and (4), we have:

$$M(g) + \frac{1}{2}O_2 \rightleftharpoons MO(s) \tag{5}$$

$$\begin{aligned} \triangle^0 G^5 &= RT\ln(P_{O_2}^{1/2}) + RT\ln(P_M) \\ \mu(O) &= \triangle^0 G^5 - RT\ln(P_M) \end{aligned} \tag{6}$$

At equilibrium, such specimens contained oxygen at the same partial pressure as that given by the known equilibrium between the alkaline or earth metal and its oxide. The oxygen content was later determined by analyzing the weight increase of the samples and by measuring the change in lattice parameter (which was compared against standards of known composition). By using two different techniques to measure this oxygen content it was possible to obtain highly reliable sets of data.

2.2.3 *The* $(HCP + \gamma\ ZrO_{2-x})$ *and* $(Liquid + \gamma\ ZrO_{2-x})$

Phase Fields. The $(HCP+\gamma\ ZrO_{2-x})$ and $(Liquid+\gamma\ ZrO_{2-x})$ phase fields are probably the two best studied regions in the Zr-O system. Ackerman et al [19] investigated the vaporization behavior of the system,Zr(s,l)+$\gamma\ ZrO_{2-x}$ over the $1627°C$ - $2227°C$ temperature range. In their experiments, a mixture of $\gamma\ ZrO_{2-x}$ and Zr metal with the overall composition $ZrO_{1.4}$[2] was set to equilibrate at different temperatures. By using mass effusion in combination with mass-spectrometric techniques, they were able to measure the partial pressure of the gaseous species $Zr(g)$,$ZrO(g)$,$ZrO_2(g)$ and $O(g)$. The oxygen chemical potential within the $(HCP + \gamma\ ZrO_{2-x})$ and $(Liquid + \gamma\ ZrO_{2-x})$ two-phase fields were obtained from the reported values for the vapor pressures of $ZrO(g)$ and $Zr(g)$ and the partial pressure of these gases measured in the effusion experiments:

For the reaction

$$ZrO(g) \rightleftharpoons Zr(g) + \frac{1}{2}O_2(g) \tag{7}$$

we have:

$$\triangle^0 G^7 = -RT\ln(P^{1/2}_{O_2(g)}) - RT\ln(P_{Zr(g)}) + RT\ln(P_{ZrO(g)}) \tag{8}$$

and

$$\mu(O) = -\triangle^0 G^7 - RT\ln(P_{Zr_g}) + RT\ln(P_{ZrO_g}) \tag{9}$$

In their work, Ackerman et al [19]also calculated the Gibbs free energy of formation for sub-stoichiometric $\gamma\ ZrO_{2-x}$ at the $(HCP + \gamma\ ZrO_{2-x})$ and $(Liquid + \gamma\ ZrO_{2-x})$ phase fields using the following reaction:

$$\gamma\ ZrO_{2-x}(s) + (1-x)Zr(g) \rightleftharpoons (2-x)ZrO(g) \tag{10}$$

Thus, we have:

$$\begin{aligned} &\triangle^0 G^{10} = -RT\ln(P^{2-x}_{ZrO(g)}) + RT\ln(P^{1-x}_{Zr(g)}) + RT\ln(a_{ZrO_{2-x}(s)}) \\ &\text{where} \\ &\triangle^0 G^{10} = (2-x)^0 G_{f,ZrO(g)} - (1-x)^0 G_{f,Zr(g)} - {}^0 G_{f,ZrO_{2-x}(s)} \end{aligned} \tag{11}$$

Assuming unit activity for the sub-stoichiometric zirconia phase and using the experimental partial pressures for both $Zr(g)$ and $ZrO(g)$, combined with the free energies of formation for $Zr(g)$ and $ZrO(g)$ obtained from JANAF Thermo-chemical Tables it was possible to obtain the free energies of formation of sub-stoichiometric $\gamma\ ZrO_{2-x}$. The values obtained in this work differed from those obtained by Ackerman et. al [19] by about 5%, which is explained by the use of different values for the vapor pressures and Gibbs free energies of formation of the different species involved in the reactions.

2.2.4 *The* $\gamma\ ZrO_{2-x}$ *phase field*

E. G. Rauh and S. P. Garg [20] studied the congruent vaporization in the $\gamma\ ZrO_{2-x}$ system over the temperature range $2077 - 2587°C$. By using mass effusion and spectrometric techniques it was possible to measure the partial pressures of both $ZrO_2(g)$ and $ZrO(g)$ over the samples with overall compositions of $ZrO_{1.98}$, $ZrO_{1.96}$, $ZrO_{1.84}$, $ZrO_{1.74}$.

From the reaction

$$ZrO_2(g) \rightleftharpoons ZrO(g) + \frac{1}{2}O_2(g) \tag{12}$$

the oxygen chemical potential, $\mu(O)$ can be obtained:

$$\mu(O) = -\triangle^0 G^{12} + RT\ln(P_{ZrO_2(g)}) - RT\ln(P_{ZrO(g)}) \tag{13}$$

[2]This composition lies within the $(HCP + \gamma\ ZrO_{2-x})$ and the $(Liquid + \gamma\ ZrO_{2-x})$ phase field.

In a similar way, from reaction

$$\gamma\ ZrO_{2-x,s} \rightleftharpoons (1-x)ZrO_{2,g} + xZrO_g \tag{14}$$

and the standard Gibbs energy of formation for the substoichiometric zirconia phase ZrO_{2-x}:

$${}^0G_{f,\gamma\ ZrO_{2-x}} = (1-x)\left[{}^0G_{f,ZrO_{2,g}} + RT\ln(p_{ZrO_2})\right] + x\left[{}^0G_{f,ZrO_g} + RT\ln(p_{ZrO})\right] \tag{15}$$

2.3 Validity of the Experimental Data

Wang and Olander [21] developed a full spectrum of the oxygen chemical potential for the *Zr-O* system. Even though the thermochemical properties of the Zr-O system have not been assessed in the entire composition and temperature range, it is possible to use thermodynamically consistent techniques to extrapolate these properties to regions in the Zr-O system that have not been explored. One such technique is the *integral constraint* [22]. Using this approach, the integral Gibbs free energy of formation of the oxide MO_C for the reaction

$$M + \frac{C}{2}O_2(g, 1\ atm) = MO_C$$

can be related to the partial molar free energy of oxygen [3],($\mu(O)$),over the whole range of compositions by

$${}^oG_{f\,MO_C} = \int_0^C \mu(O); dC \tag{16}$$

where C is the $\frac{O}{M}$ ratio. (16) is basically a generalization of the *Gibbs-Duhem* relation.

Wang and Olander used the phase boundary values reported by Abriata [6]; the enthalpies of solution of oxygen in the BCC and the $(BCC + HCP)$ phase fields [16]; data on the chemical potential of oxygen in the $(HCP + \gamma\ ZrO_{2-x})$ phase field and Gibbs free energies of formation of $\gamma\ ZrO_{2-x}$ [19] and applied Eq. (16):

$$\begin{aligned} 2\frac{{}^oG_{f,\gamma\ ZrO_{C_{\gamma/H}}}}{RT} = &\int_0^{C_{B/H}} \ln(p_B); dC + \int_{C_{B/H}}^{C_{H/B}} \ln(p_{B/H}); dC \\ &+ \int_{C_{H/B}}^{C_{H/\gamma}} \ln(p_H); dC + \int_{C_{H/\gamma}}^{C_{\gamma/H}} \ln(p_{H/\gamma}); dC \end{aligned} \tag{17}$$

where $C_{X/X}$ corresponds to the $\frac{O}{M}$ *ratio* at the phase boundaries; p_X is the oxygen partial pressure (or p_{O_2}) within a single phase field and $p_{X/X}$ corresponds to the activity of oxygen within any two-phase field.

In order to obtain expressions for the oxygen chemical potentials ($RT\ln(p_{O_2})$) for the BCC, $(BCC + HCP)$ and HCP phase fields, Wang and Olander used Eq.(17) and minimized the difference between both sides of the equation (what they called *closure error*). Assuming that the *BCC* solid solution obeyed *Henry's Law* and that the oxygen partial pressure p_{O_2} in the *HCP* phase field could be linearly interpolated from the oxygen partial pressure in the surrounding two-phase fields [4] they obtained explicit expressions for the oxygen partial pressures in the $(BCC + HCP)$ and $(HCP + \gamma\ ZrO_{2-x})$ phase fields[5]. Using their approach we obtained explicit expressions

[3] with respect to $O_2(g)$

[4] $(BCC + HCP)$ and $(HCP + \gamma\ ZrO_{2-x})$

[5] Wang and Olander did not report explicit expressions for the actual oxygen partial pressure in the single-phase fields, although they graphically represented such partial pressures.

for the oxygen partial pressure in the remaining phase fields:

$$\begin{aligned}
\ln(p_{BCC}) &= -\frac{141,184}{T} + 27.03 + 2\ln(C) \\
\ln(p_{BCC/HCP}) &= \frac{-154,799}{T} + 29.66 \\
\ln(p_{HCP}) &= -\frac{136,135}{T} + 17.18 + \frac{10,610 \cdot C}{T} \\
&\quad - \frac{9.21 \times 10^6 - 1.554 \times 10^7 \cdot C - 5.62 \times 10^3 \cdot T + 10.61 \times 10^3 \cdot T \cdot C}{T^2 - 3.787 \times 10^3 \cdot T + 4.16 \times 10^6} \\
\ln(p_{HCP/\gamma\ ZrO_{2-x}}) &= -\frac{133,519}{T} + 17.18
\end{aligned} \tag{18}$$

To obtain Eqs. (18) several assumptions and simplifications were made,the validity of which was not entirely known beforehand. For example, the use of a simple linear extrapolation for determining the oxygen partial pressure within the large *HCP* phase field seems rather questionable. Additionally, the data used for estimating the thermochemical parameters comes from several sources and some of the experimental data had not been independently confirmed.

As was noted above, Komarek and Silver [18] measured the thermochemical properties (partial molar free energies, enthalpies and entropies) of *HCP* Zr-O solid solutions between the ranges $800°C$ to $1000°C$ by equilibrating thin zirconium specimens with alkaline earth-metal vapors of known oxygen partial pressure.

We tested the expression for the oxygen partial pressure in the HCP phase field (third equation in Eqs. (18)) against the independent experimental results obtained by [18] and found that not only the validity of all the assumptions made by Wang and Olander can be justified, but the consistency between all the experimental data used can be proved:

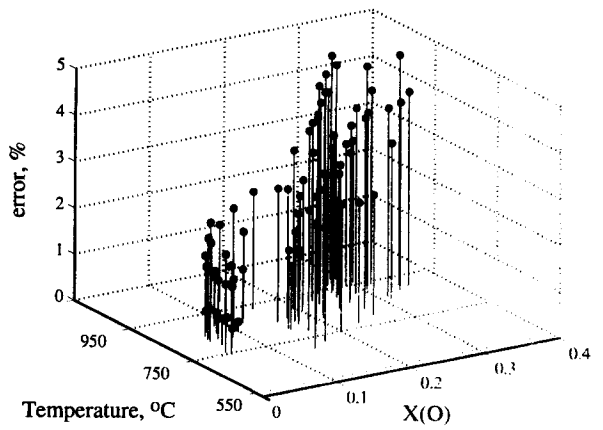

Figure 1: The error (absolute value) between the data by Komarek at al [18] and the expression for the oxygen partial pressure in *HCP* found in Eq. (18)

Fig. 1 shows that there is good agreement between the expression obtained for $RT\ln(p_{O_2})_{HCP}$ and the data

obtained by [18], the average error being only 2.61%. The fact that the error between an independent set of experimental data and the expression for the oxygen chemical potential within the HCP phase field is small proves the consistency of all the data used for the analysis, including both phase diagram and thermochemical information.

Although it is true that by using the *CALPHAD* approach it is possible to detect inconsistencies in thermochemical or phase diagram data, the fact that the validity of the thermochemical data can be verified apriori results very useful, especially when assessing the relative weight that each experimental data point should have in the optimization of the parameters of the model.

3 Thermodynamic Models

3.1 Gas Phase

To calculate the oxygen-rich side of the *Zr-O* phase diagram, the gas phase had to be considered. The ideal gas model was used, considering the following species:

$$(O, O_2, O_3, Zr, Zr_2, ZrO, ZrO_2)$$

The Gibbs free energy of this phase would be given by:

$$\begin{aligned} G_m^{Gas} = & x_O \left({}^0G_O + RT\ln(P)\right) + x_{O_2} \left({}^0G_{O_2} + RT\ln(P)\right) + x_{O_3} \left({}^0G_{O_3} + RT\ln(P)\right) \\ & + x_{Zr} \left({}^0G_{Zr} + RT\ln(P)\right) + x_{Zr_2} \left({}^0G_{Zr_2} + RT\ln(P)\right) \\ & + x_{ZrO} \left({}^0G_{ZrO} + RT\ln(P)\right) + x_{ZrO_2} \left({}^0G_{ZrO_2} + RT\ln(P)\right) \\ & + RT\left(x_O\ln(x_O) + x_{O_2}\ln(x_{O_2}) + x_{O_3}\ln(x_{O_3})\right) \\ & + RT\left(x_{Zr}\ln(x_{Zr}) + x_{Zr_2}\ln(x_{Zr_2})\right)) \\ & + RT\left(x_{ZrO}\ln(x_{ZrO}) + x_{ZrO_2}\ln(x_{ZrO_2})\right)) \end{aligned} \tag{19}$$

where ${}^0G_s$ is the standard Gibbs energy of species s and x_s is the molar fraction of species s in the ideal gas mixture.

3.2 Liquid Phase

The liquid phase goes from pure liquid zirconium to stoichiometric liquid ZrO_2. Therefore, any model used would have to be able to represent the Gibbs free energy of the liquid phase from pure liquid zirconium to pure stoichiometric ZrO_{2-x} in a continuous manner. The ionic two-sublattice model for liquids [23] has been found to be extremely useful for this purpose:

$$\left(C_i^{+v_i}\right)_P \left(A_j^{-v_j}, Va, B_k^0\right)_Q$$

where $C_i^{v_i}$ corresponds to the $cation_i$ with valence $+v_i$; A_j to the $anion_j$ with valence $-v_j$; *Va* are hypothetical vacancies added to ensure electro-neutrality when the liquid departs from stoichiometry [6], having a valence equal to the average charge of the *cations* Q ; and finally B_K^0, which represents any neutral component dissolved in the liquid.

The number of sites in the sublattice, P and Q are varied in such a way that electro-neutrality for all compositions is ensured:

$$P = \sum_j v_j y_{A_j} + Q\, y_{Va} \tag{20a}$$

$$Q = \sum_i v_i y_{C_i} \tag{20b}$$

[6] i.e. when the system approaches the metallic-rich composition range

where y_x corresponds to the sublattice fraction of component x in its sublattice.

For the particular case of the Zr-O system, this two-sublattice model is simply:

$$\left(Zr^{+4}\right)_{4-2y_{O^{-2}}}\ \left(O^{-2},Va^{-4}\right)_4$$

The Gibbs free energy expression for this system is:

$$\begin{aligned} G_m^{Liquid} &= y_{Zr^{+4}}y_{O^{-2}}\,{}^0G_{(Zr^{+4})_2(Va^{-4})_4,L} + 4y_{Zr^{+4}}y_{Va^{-4}}\,{}^0G_{(Zr^{+4})(Va^{-4})} \\ &+ RT(4-2y_{O^{-2}})\left(y_{Zr^{+4}}\ln(y_{Zr^{+4}})\right) \\ &+ RT(4)\left(y_{O^{-2}}\ln(y_{O^{-2}}) + y_{Va^{-4}}\ln(Va^{-4})\right) \\ &+ G_m^{ex} \end{aligned} \tag{21a}$$

$$G_m^{ex} = y_{Zr^{+4}}y_{O^{-2}}y_{Va^{-4}}\sum_{k=0}^{k}{}^kL_{(Zr^{+4}:O^{-2},Va^{-4})}(T)\left(y_{O^{-2}}-y_{Va^{-4}}\right)^k \tag{21b}$$

where ${}^0G_{(Zr^{+4})_2(Va^{-4})_4,L}$ corresponds to the standard Gibbs free energy for two moles of ZrO_2, L; ${}^0G_{(Zr^{+4})(Va^{-4})}$ is the standard Gibbs free energy of pure *Liquid* zirconium and ${}^kL_{(Zr^{+4}:O^{-2},Va^{-4})}$ corresponds to the excess chemical interaction parameters between oxygen and vacancies in the second sub-lattice. This last parameter is identical to a *Redlich-Kister* polynomial.

The advantage of using the ionic sub-lattice model is that it can be easily coupled to higher order systems, so ternary liquid phases involving *zirconium* and *oxygen* can be easily modelled.

3.3 BCC and HCP Phases

It is well-known that the stable solid phases of zirconium (BCC and HCP) disolve oxygen interstitially into their octahedral interstitial sites [11]. The solid solutions of *Zr-O* can be represented with the two-sublattice formalism, with one sublattice occupied by zirconium atoms and the other one occupied by both oxygen and vacancies:

$$(Zr)_1\,(O,Va)_c$$

where c corresponds to the ratio of interstitial sites to normal sites in each structure.

For the BCC phase, the stoichiometry ratio c is equal to 3. For the HCP phase, we decided to use the stoichiometry ratio used for the very similar *HCP Ti-O* phase [24], i.e. $c=\frac{1}{2}$. It is important to note that using this stoichiometry ratio, it is impossible for the model to show the maximum oxygen solubility limit at the eutectic point of $\sim 35at.\%$[7]. However, high priority was given to the compatibility of this model with the models available for other systems (such as *Ti-O*), and c was fixed to meet this requirement. Using the sublattice formalism [25] we have:

$$G_m^{HCP,BCC} = y_O\,{}^0G_{ZrO_c} + y_{Va}\,{}^0G_{ZrVa_c} + cRT\left(y_O\ln(y_O)+y_{Va}\ln(y_{Va})\right) + G_m^{ex} \tag{22a}$$

$$G_m^{ex} = y_Oy_{Va}\sum_{k=0}^{k}{}^kL_{(Zr:O,Va)}(T)\left(y_O-y_{Va}\right)^k \tag{22b}$$

where ${}^0G_{ZrO_c}$ is the standard Gibbs free energy of the *hypothetical* oxide ZrO_c, which is one of the end members that establishes the reference surface for this model; ${}^0G_{ZrVa_c}$ corresponds to the standard Gibbs free energy of the pure BCC or HCP phases and the chemical interaction for the oxygen and vacancies in the second sublattice is given by $\sum_{k=0}^{k}{}^kL_{(Zr:O,Va)}(T)\left(y_O-y_{Va}\right)^k$.

[7]The fact that the maximum oxygen solubility in $HCP-Zr$ is greater than that observed in the equivalent phases in the *Ti-O* and *Hf-O* systems can be explained by considering that the c-axis of the $HCP-Zr$ unit cell ($.515nm$) is greater than those for $HCP-Ti$ ($.468nm$) and $HCP-Hf$ ($.505nm$). Therefore, there is more space available for oxygen to dissolve interstitially in the *HCP-Zr* phase, specially at the high temperatures close to the eutectic point [11].

3.4 The Ordered HCP Interstitial Solutions

In binary interstitial alloys, the solubility of interstitial elements into metals is usually so low that interstitial ordering is not observed. However, the HCP phases of $IV\ A$ transition elements dissolve large amounts of oxygen in their octahedral interstitial sites. In all these systems, a tendency for ordering has been observed in the low temperature, high oxygen content region of the phase diagram. Except for some x-ray diffraction experiments, there is virtually no information on the nature of these phases in the *Zr-O* system and the reported phase boundaries between these highly ordered interstitial phases and the surrounding HCP are rather speculative [6]. Because these ordered phases occur at such low temperatures, (below $500°C$), equilibration experiments are difficult to perform and therefore, all the information available has to be taken cautiously. For this work, the phases Zr_6O, Zr_3O and Zr_2O were modelled as stoichiometric compounds,

$$(Zr)_c\,(O)$$

For these phases, the Gibbs free energy of formation would be given by:

$${}^0G_{f,Zr_cO} = \triangle H_{f\,Zr_cO} - T\,\triangle S_{298,Zr_cO} \tag{23}$$

3.5 The ZrO_{2-x} Phases

The ZrO_{2-x} compound can exist, at $1\ atm.$, in three different structural modifications. The low-temperature phase, $\alpha\ ZrO_{2-x}$, has a monoclinic structure and has been reported to exhibit a certain degree of non-stoichiometry. It has been observed that under reducing conditions, the predominant defects are ionized vacancies [26]. The medium-temperature tetragonal phase,$\beta\ ZrO_{2-x}$ (prototype: HgI_2), has a higher degree of non-stoichiometry [27]. In this phase, it has been observed that under reducing conditions, oxygen vacancies are the predominant defects. For these two phases, it has been reported that at high oxygen partial pressures, a further oxidation of the structure(zirconium deficiency), i.e. ZrO_{2+x} is observed [26]. However, no conclusive evidence exists and this fact was ignored in the development of the model. Although there is information regarding phase boundaries and thermochemical properties of the high-temperature cubic phase,$\gamma\ ZrO_{2-x}$ (prototype: CaF_2), there is virtually no information on the defect structure of this phase. This phase presents a large degree of non-stoichiometry and is stable at temperatures far lower than the $\beta \rightarrow \alpha$ transformation temperature for the stoichiometric phases. There are however, some other non-stoichiometric oxide systems that present large degrees of non-stoichiometry and for which a defect structure has been established, CeO_{2-x} being one example [28]. For these other oxide phases, vacancies have been used to successfully model their thermochemical properties under reduction conditions. Therefore, we consider that for the $\gamma\ ZrO_{2-x}$ phase, vacancies can be considered to be the primary defect.

For these three phases, the formation of defects can be understood using the following reaction:

$$O^{-2}_{lattice} \rightleftharpoons \frac{1}{2}O_{2,g} + Va + 2e^-$$

According to this equation, the reduction of the zirconia phase involves the formation of an oxygen vacancy plus two free electrons. In fact, experiments have shown that under reducing conditions, both the monoclinic and tetragonal phases change their color from white to gray or black, indicating the presence of conduction electrons [29]. Despite this fact, it has been shown that a satisfactory description of the non-stoichiometry and its relationship to oxygen potentials is possible without considering conduction electrons [24]. In their work on the Titanium-Oxygen system, Waldner and Eriksson [24] used a two sublattice model to describe the fluorite-type TiO_{2-x} phase. In this work, we use the same description, giving the oxygen vacancy a double negative charge to maintain electro-neutrality of the phase:

$$\left(Zr^{+4}\right)_1\left(O^{-2}, Va^{-2}\right)_2$$

For this model, the Gibbs free energy expression would be:

$$G_m^{ZrO_2} = y_{O^{-2}}\,{}^0G_{ZrO_2} + y_{Va^{-2}}\,{}^0G_{ZrVa_2} + 2RT\left(y_{O^{-2}}\ln(y_{O^{-2}}) + y_{Va^{-2}}\ln(y_{Va^{-2}})\right) + G_m^{ex} \tag{24a}$$

$$G_m^{ex} = y_{O^{-2}} y_{Va^{-2}} \sum_{k=0}^{k} {}^{k}L_{(Zr:O,Va)}(T)\,(y_{O^{-2}} - y_{Va^{-2}})^k \tag{24b}$$

For the implementation of this model, it was necessary to assign a value for the standard Gibbs energy for the $ZrVa_2$ compound, which corresponds to the lattice energy of *zirconium* in the monoclinic, $HgI2$ and CaF_2 structures. This free energy was *arbitrarily* set to be 200,000 J/mol less stable than the stable *HCP* phase. The α ZrO_{2-x} low-temperature zirconia phase shows negligible non-stoichiometry, therefore, the chemical interaction parameters, $\sum_{k=0}^{k} {}^{k}L_{(Zr:O,Va)}(T)\,(y_{O^{-2}} - y_{Va^{-2}})^k$ were set to 0.

It is important to note that this model results in a $p_{O_2} \propto x^{-1/2}$ relationship at low oxygen partial pressures. For the β ZrO_{2-x} phase, experimental data [29] show this relationship to be $p_{O_2} \propto x^{-1/6}$ at high temperatures ($T > 1400°C$) and decreases to $p_{O_2} \propto x^{-1/2}$ at lower temperatures. Thus, for the β ZrO_{2-x} phase, a more complicated model would have to be used. However, experimental data are lacking and therefore it was decided that the simple two-sublattice model was to be used for all three substoichiometric phases.

4 Model Optimization and Comparison with Experimental Results

The parameters needed for the description of the Gibbs Free Energy expressions describing all the phases present (except for the highly ordered, HCP-based interstitial solutions and the Gas phase) were optimized using the *PARROT* subroutine of the Thermo-Calc Software mentioned earlier. Values for the Gibbs free energies of the pure components and the free energies of formation for the stoichiometric oxides ZrO_2 were obtained from the SGTE and the *JANAF Thermochemical Tables*. The different sets of experimental thermochemical and phase diagram data were assigned different statistical weights during the optimization according to the accuracy reported in the original papers and the consistency with respect to the calculated phase diagram.

4.1 Comparison with Phase Diagram Data

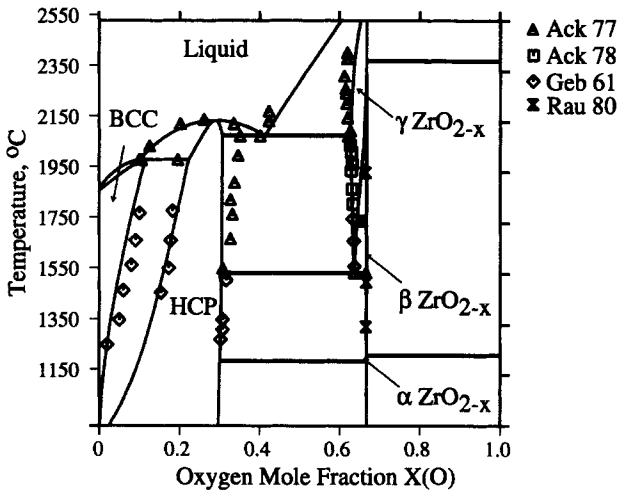

Figure 2: Experimental data vs. calculated phase diagram. Experimental data obtained from [7], [14], [13] and [10]

As can be seen in Fig. 2 and Table 1, the experimental and calculated phase diagram data agree rather well, except for some minor discrepancies:

Table 1: Comparison between Calculated and Experimental Invariant Points in the Zr-O system.

Reaction	$at.\%O$ of Respective Phases			Temp. ^oC	
$L + (HCP) \rightleftharpoons BCC$	10.0 ± 0.5	19.5 ± 2	10.5 ± 0.5	1970 ± 10	Exp.
	10.03	22.17	10.5	1977	Calc.
$L \rightleftharpoons HCP + \gamma\ ZrO_{2-x}$	40 ± 2	35 ± 1	62 ± 1	2062 ± 10	Exp.
	41.22	31.1	62.54	2074	Calc.
$\gamma\ ZrO_{2-x} \rightleftharpoons$	63.6 ± 0.4	31.2 ± 0.5	66.5 ± 0.1	~ 1525	Exp.
$HCP + \beta\ ZrO_{2-x}$	63.49	30.41	66.5	1530	Calc.
$L \rightleftharpoons HCP$		25.0 ± 2		2130 ± 10	Exp.
		27.5		2127.8	Calc.

- The $BCC/(HCP + BCC)$ phase boundary calculated in this work presents an oxygen solubility slightly lower than that presented in the literature [10].
- One of the major discrepancies between the experimental information and the calculated phase diagram is the maximum solubility of oxygen within the HCP phase ($35\ at.\%\ vs.31\ at.\%$). As was noted above, the model used to describe the HCP phase is unable to represent the experimental maximum solubility (the theoretical maximum obtained using the $(Zr)\ (O, Va)_{0.5}$) model is just $33\ at.\%$. However, it is important to consider that there is only one set of experimental data points that describes the eutectic point [7] which in reality is an extrapolation of the $HCP/(HCP + \gamma\ ZrO_{2-x})$ phase boundary points obtained at lower temperatures (which agree well with the calculated diagram) and therefore the actual value for this maximum solubility may be lower than the one reported.
- Another major discrepancy is the composition at which the HCP melts congruently. The calculated value is $2at.\%$ higher than that reported in the literature. Given the fact that in similar transition metal-oxide systems, namely *Ti-O*, this composition is rather close to the maximum solubility composition [24], hence there are reasons to believe that the congruent melting composition should be on the high side of the uncertainty range reported.
- The retrograde solubility observed in the lower $Liquid/(Liquid + \gamma\ ZrO_{2-x})$ phase boundary was not reproduced in the present work, but given the experimental uncertainties reported [7] we consider that the agreement is satisfactory.

4.2 Comparison with Thermochemical Data

Fig. 3 shows the calculated and experimental [16], [17] partial molar enthalpies of oxygen ($\Delta\overline{H}(O_2)$) within the BCC,$(BCC+HCP)$ and HCP phase fields. In general, good agreement was obtained, having a maximum error of 12% at low oxygen concentrations. It is worth noting that both the model and the experimental data show that the enthalpy of solution of oxygen in the $(BCC + HCP)$ region is more negative than the enthalpy of solution within the BCC phase field. If *Henry's Law* is followed up to the maximum oxygen solubility in the BCC phase, we have

$$\frac{1}{\gamma_O^0} = \frac{X_O}{\sqrt{p_{O_2,BCC}}} = \frac{X_{O,sat}}{\sqrt{p_{O_2,BCC/HCP}}}$$
$$2\ \mu(O)_{BCC} = 2\ \mu(O)_{BCC/HCP} + 2\ RT \ln(\frac{X_O}{X_{O,sat}}) \tag{25}$$

where $p_{O_2,BCC}$ is the oxygen pressure within the *BCC* phase; $X_{O,sat}$ is the maximum solubility of oxygen in the *BCC* phase; $p_{O_2,BCC/HCP}$ is the oxygen pressure within the $(BCC + HCP)$ phase fields; and $\mu(O)_{BCC}$ and

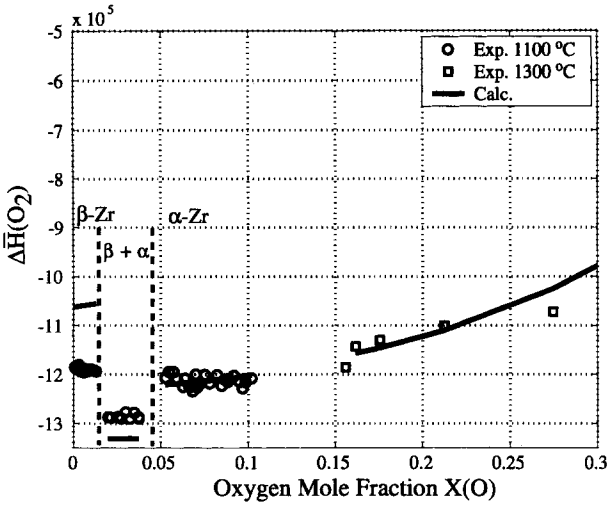

Figure 3: Experimental [17], [16] vs. calculated partial molar enthalpies of oxygen, $\triangle\overline{H}_{O_2}$, within the BCC,$(BCC + HCP)$ and HCP phase fields.

$\mu(O)_{BCC/HCP}$ are the oxygen chemical potentials within the *BCC* and $(BCC + HCP)$ phase fields respectively.

The partial molar enthalpy of oxygen within the BCC phase can be obtained:

$$\triangle\overline{H}_{O_{2,BCC}} = \frac{\partial\left(\frac{2\,\mu(O)_{BCC/HCP}}{T}\right)}{\partial[1/T]} = \triangle\overline{H}(O_2)_{BCC/HCP} + 2RT^2\frac{dX_O/dT}{X_O} \tag{26}$$

Since $dX_O/dT > 0$, it is obvious that $\triangle\overline{H}(O_2)_{BCC}$ must be more positive than $\triangle\overline{H}(O_2)_{BCC/HCP}$. The model and the experimental data agree well and show that *Henry's Law* is obeyed in the *BCC* phase.

From Fig. 3 it can also be seen that $\triangle\overline{H}(O_2)_{HCP}$ remains almost constant up to $15\,at.\%$. After this composition, the molar partial enthalpy starts to increase rather sharply. This behavior has been observed for the *Ti-O* system and is consistent with the presence of low-temperature ordered structures [16].

Fig. 4 shows the absolute percent difference the experimental [18] and calculated $\mu(O)$ within the HCP phase field. Below $30\,at\%\ O$ there is relatively good agreement between the extensive experimental information and the calculated properties. However, when the composition approaches the solubility limit, the error increases noticeably. Near this solubility limit, Komarek and Silver observed that a black layer, probably oxygen-deficient ZrO_2 was formed at the surface of the samples. Although they did not detect any weight changes, the presence of this layer may have hindered the oxidation of the metallic samples and thus affected the final compositions measured. Therefore, these experimental data should have a lower statistical weight than the ones obtained at lower oxygen concentrations.

Fig. 5 shows the data obtained by Ackerman et al [19] on the oxygen chemical potential $\mu(O)$ (Ref. State: $O_2(g)$) within the $(HCP + \gamma\ ZrO_{2-x})$ and $(Liquid + \gamma\ ZrO_{2-x})$ phase fields, together with the values calculated using the model developed in this work. As can be seen, the agreement is rather good, with the error close to $10\,at.\%$. The temperature dependence (entropy) of the chemical potential using the model is almost identical to the one obtained from experiments.

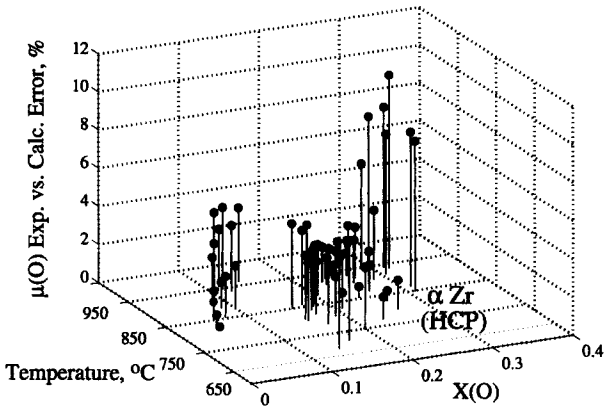

Figure 4: Absolute percent difference between experimental [18] and calculated oxygen chemical potential,$\mu(O)$, within the HCP phase.

Fig. 6 shows good agrement between the experimental and calculated standard Gibbs energy of formation for the γ ZrO_{2-x} high-temperature zirconia phase. As expected, the stoichiometric phase should be more negative than the sub-stoichiometric phase. The experimental points were calculated using Ackerman et. al [19] mass spectroscopy measurements, together with the phase boundary data obtained in [7]. The peak observed in the experimental ${}^{0}G_{f,\gamma\ ZrO_{2-x}}$ curve is due to the retrograde solubility as measured by [7]. This was not reproduced using the present model and therefore in this temperature range, the discrepancies between experiments and calculations are greater. As expected, ${}^{0}G_{f,\gamma\ ZrO_{2-x}}$ is more negative than $\frac{2-x}{2}{}^{0}G_{f,\gamma\ ZrO_2}$. This leads to a negative

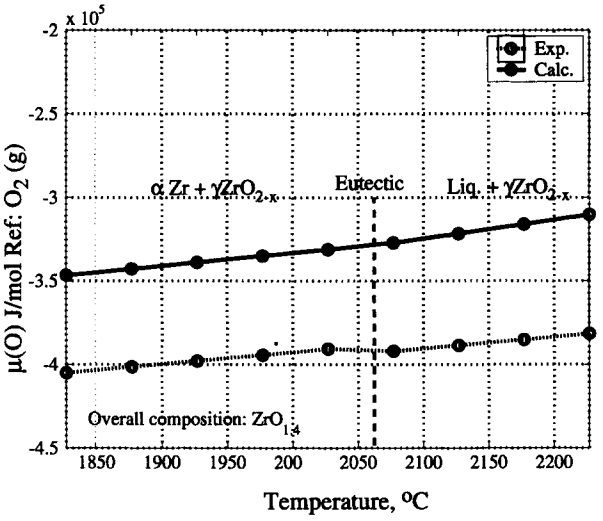

Figure 5: Experimental [19] and calculated oxygen chemical potential,$\mu(O)$, within the $(HCP + \gamma\ ZrO_{2-x})$ and $(Liquid + \gamma\ ZrO_{2-x})$ phase fields

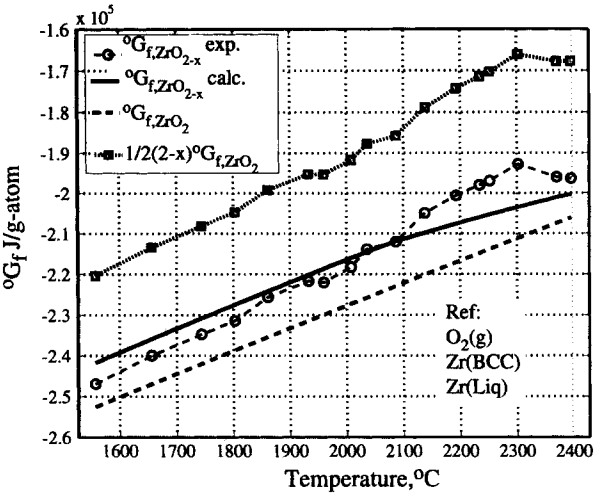

Figure 6: The standard Gibbs energy of formation of $\gamma\ ZrO_{2-x}$, ${}^0G_{f,\gamma\ ZrO_{2-x}}$, (experimental [19] and calculated) at the lower phase boundary-$Liquid/(Liquid + \gamma\ ZrO_{2-x})$-per mole of atoms. Comparison with ${}^0G_{f,\gamma\ ZrO_2}$ and $\frac{2-x}{2}{}^0G_{f,\gamma\ ZrO_2}$.

Gibbs energy change for the reaction [19]:

$$\frac{2-x}{2}ZrO_2(s) + \frac{x}{2}Zr(s) \rightharpoonup ZrO_{2-x}(s) \tag{27}$$

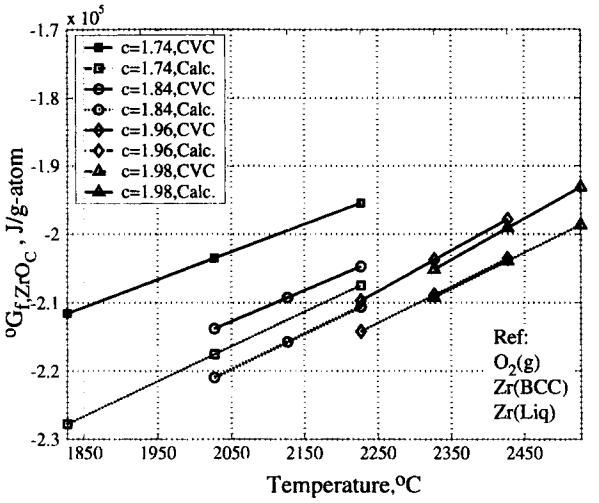

Figure 7: The standard Gibbs energy of formation,${}^0G_{f,ZrO_c}$, of $\gamma\ ZrO_c$ at different temperatures. *CVC* corresponds to the values obtained from the analysis of the data obtained by Rauh and Garg [20]from congruent vaporization experiments. *Calc* corresponds to the values calculated using the model developed in this work.

In order to obtain the absolute value for the zirconium partial pressure within the two-phase field, Ackerman et al [19] developed a technique for the direct measurement of the activity of zirconium in that region of the *T-x* diagram. A pure zirconium sample was placed in contact with a pure ZrO_2 disc at 1827^oC. The combined composition was set to $ZrO_{1.4}$, which lies within the two-phase field. They monitored the ion current for Zr (I_{Zr^+}) until a steady-state condition was reached.

According to their observations, the ratio of the steady-state ($ZrO_{1.4}$) and initial (pure zirconium) ion currents corresponds to the activity of zirconium within the two-phase field at 1827^oC. This activity was measured to be 0.68, having pure zirconium at 1827^oC as the reference state. Our model predicts that under this conditions, the activity of Zirconium must be 0.29. Given the fact that our model is able to predict with great accuracy the direct oxygen partial pressure measurements by Komareck et al [18], we believe that the measurement of the activity using mass spectroscopic techniques is faulty. One possibility is that equilibrium was not reached due to the formation of oxide scales in the zirconium sample (Komareck et al [18] observed this behavior in their experiments). The calculated and experimental values for the Gibbs energy of formation of $G_{ZrO_{2-x}}$ within the two-phase field are not affected by this discrepancy in the activity of Zr, since the ratio $\frac{p_{ZrO}}{p_{Zr}}$ and not the absolute values of p_{ZrO} and p_{Zr} are important in Eq. (11)).

In their congruent vaporization experiments Rauh and Garg [20] measured directly the relative ionic intensities for the species $ZrO_{2,g}$ and ZrO_g. through mass spectrometric techniques. From Eq. (15) the standard Gibbs energy of formation of the substoichiometric zirconia phase γ ZrO_{2-x} can be easily calculated (assuming unit activity for the substoichiometric phase). Fig. 7 shows that the values calculated by Rau [20] and the ones obtained with our model agree rather well.

4.3 Comparison between the Present Model and the Thermochemical Functions obtained using the Integral Constraint Approach

As described above, Wang and Olander [21] assessed the validity of the available thermochemical data for the *Zr-O* system and simultaneously obtained expressions for the thermochemical partial properties of oxygen within the phase fields for which thermochemical data were lacking or were not reliable. Fig. 1 proves the self-consistency of the thermochemical and phase diagram data used by Wang and Olander. It would then be useful to compare their results to those obtained by our model.

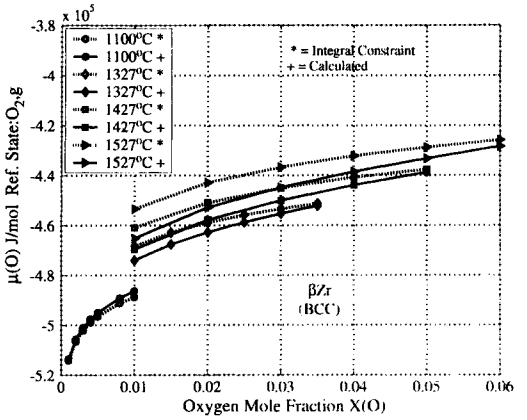

Figure 8: Oxygen chemical potential,$\mu(O)$, within the BCC phase. Comparison between the model obtained in this work and the one obtained by Wang and Olander [21].

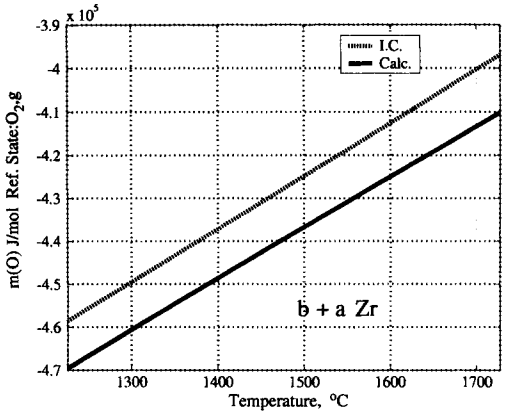

Figure 9: Oxygen chemical potential,$\mu(O)$, within the $(BCC + HCP)$ phase field. Comparison between the model obtained in this work and the one obtained by Wang and Olander [21].

As can be seen in Figs. 8 and 9, the agreement between the thermochemical properties calculated using this model and the one obtained by Wang and Olander is good. The fact that both models (one analytical, the other one using the sub-lattice formalism) yield relatively similar results is encouraging, since this confirms the validity of both the data used for the optimization and the model used to describe the main phases in the *Zr-O* system.

4.4 Modelling of the Ordered Interstitial Phases

Since there is very little information regarding the nature of the ordered interstitial phases at the high-oxygen, low-temperature region of the HCP phase field, we decided to model these as three stoichiometric compounds,Zr_6O, Zr_3O and Zr_2O. Because there is no thermodynamic data on these phases, simple estimations were used:

Kubaschewski et. al [30] report a simple formula for the estimation of the enthalpy of formation of ionic compounds:

$$^0\Delta\overline{H}_{MO_c} = -96390.8(2c)\,(\epsilon_M - \epsilon_O)^2 \tag{28}$$

where $2c$ corresponds to the number of ionic bonds, and ϵ_M and ϵ_O correspond to the Pauling's electro-negativities. For this particular case, $\epsilon_{Zr} = 3.44$ and $\epsilon_O = 1.33$.

Table 2: Comparison between calculated and experimental/assessed enthalpies of formation $(J/g - atom)$ for the compounds ZrO_2, ZrO_3 and $ZrO_{0.5}$.

Compound	Electronegativities	Experimental/Assessed	Corr. Factor
ZrO_2	-0.573×10^6	-0.366×10^6	63.8%
ZrO_3	-0.644×10^6	-0.411×10^6	63.8%
$ZrO_{0.5}$	-0.286×10^6	-0.217×10^6	75.0%

Table 2 shows the comparison between the experimental/assessed data for three *Zr-O* compounds (The enthalpies of formation for the hypothetical compounds $ZrO_{0.5}$ and ZrO_3 were determined during the assessment). Using the sublattice model for the solid solution phases HCP and BCC (See Eq. (22)), it can be shown that:

$$G_{ZrO_c} = {}^0G_{ZrO_c} + cRT\ln(y_O) + (1-2y_O)^2\left[{}^0L_{O,Va} + \sum_1^n {}^kL_{O,Va}\,(2y_O-1)^{k-1}\,((2k+1)\,y_O - 1)\right] \tag{29}$$

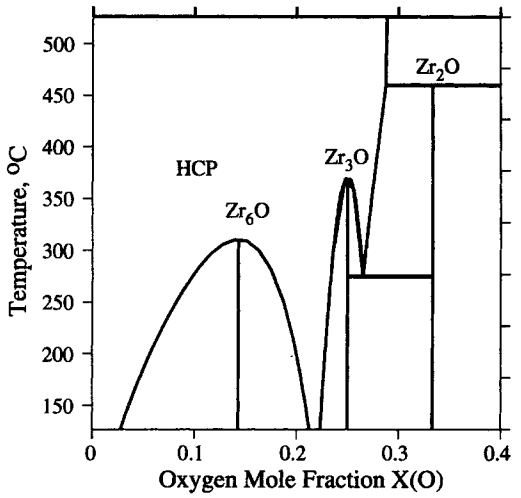

Figure 10: Interstitial Low-Temperature Phases. Highly Hypothetical

The zeroth-order interaction parameter ${}^0L_{O,Va}$ can thus be 'lumped' into the expression for the Gibbs energy of formation of the ZrO_c compound,${}^0G_{ZrO_c}$. In table 2, the assessed enthalpies of formation for the ZrO_c compounds are thus given by:

$$ {}^0\Delta\overline{H}_{ZrO_c} = \frac{\partial\frac{({}^0G_{ZrO_c}+{}^0L_{O,Va})}{T}}{\partial[1/T]} \tag{30} $$

The optimization of the Gibbs energy of formation of the interstitial phases began by using Eq. (28) and then applying an average correction factor of 70% (See Table 3). The value for the entropy of formation was obtained by fixing the temperature at which each of the interstitial compounds would become unstable ($T \sim 297°C$, $T \sim 377°C$ and $T \sim 427°C$ for the compounds Zr_2O, Zr_3O and Zr_2O, respectively). Further adjustments were made to the parameters, since the Gibbs energy of the *HCP* phase affected the relative stability of the stoichiometric phases.

Table 3: Comparison between calculated (using Eq. (28)) and assessed enthalpies of formation ($J/g-atom$) for the compounds Zr_6O, Zr_3O and Zr_2O.

Compound	Electronegativities	Experimental/Assessed	Corr. Factor
Zr_6O	-0.122×10^6	-0.093×10^6	76.2%
Zr_3O	-0.214×10^6	-0.151×10^6	70.5%
Zr_2O	-0.286×10^6	-0.198×10^6	69.2%

Fig. 10 shows the calculated ordered interstitial phases. Note that this description does not correspond to the real nature of these phases, since no ordering model was used. The values obtained for the Gibbs energies of formation of the stoichiometric compositions could be used as starting points for future assessments in which long-range and/or short-range ordering is considered.

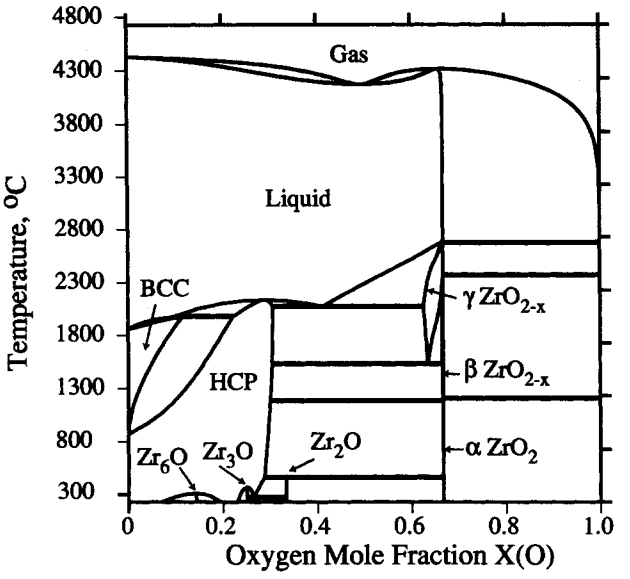

Figure 11: Calculated Phase Diagram

4.5 Calculated Phase Diagram over the entire Compositional and Temperature Ranges

Fig. 11 shows the calculated phase diagram over the entire compositional and temperature ranges. It can be observed that the model was able to calculate the equilibrium ($CondensedPhases + Gas$) phase fields. In general, good agreement was observed between experimental and calculated phase diagram data. The invariant points and phase boundaries calculated using the model developed in this work agree well with the experimental determinations.

5 Conclusion

Several sets of thermochemical and phase diagram data (invariant points and phase boundaries) have been used to develop a model for the *T-x* phase diagram for the *Zr-O* system. The validity of the data used for the optimization was assessed and it was found that the data were self-consistent. This was later used to assign the relative statistical weights during the parameter optimization procedure. In general, good agreement has been observed between the experimental and calculated phase diagram and thermochemical properties.

The ordered interstitial phases present in the high-oxygen, low-temperature region of the HCP phase field have been modelled as three stoichiometric compounds. Although this does not represent the true nature of the order-disorder transformations in interstitial *HCP-based* solid solutions, we believe that the Gibbs energies obtained are a good starting point for more complete optimizations.

Except for a few discrepancies at some invariant points, we have been able to obtain a model that is self-consistent and may serve as part of more complete databases for metallic and oxide systems. The incorporation of a more complete thermodynamic model into the studying of several technological applications involving the *Zr-O* system will allow a better understanding of the processes involved.

References

[1] C. S. Montros. Methodology for Analysing the Degradation of Mg-PSZ. *J. Mater. Sci.*, 27:2218–2222, 1992.

[2] L. Kindermann, D. Das, D. Bahadur, R. Weiß, H. Nickel, and K. Hilpert. Chemical Interactions between La-Sr-Mn-Fe-O-Based Perovskites and Yttria-Stabilized Zirconia. *J. Am. Ceram. Soc.*, 80:909–914, 1997.

[3] L. Kaufman and E. V. Clougherty. Thermodynamic Factors Controlling the Stability of Solid Phases at High Temperatures and Pressures. In AIME Metall. Soc., editor, *Metallurgy at High Pressures and High Temperatures*, pages 322–379, New York, 1964. Gordon and Breach, Science Publishers.

[4] B. Jansson. Evaluation of Parameters in Thermochemical Models using different types of Conditions. Technical report, Division of Metallurgy, Royal Institute of Technology, Stockholm, Sweden, 1984.

[5] B. Sundman. *User Aspects of Phase Diagrams*, page 130. Inst. Metals, London, 1991.

[6] J. P. Abriata and R. Versaci. The O-Zr (Oxygen-Zirconium) System. *Bull. of Alloy Phase Diagrams*, 7(2):116–124, 1986.

[7] R. J. Ackerman, S. P. Garg, and E. G. Rauh. High-Temperature Phase diagram for the System Zr-O. *J. Am. Ceram. Soc.*, 60:341–345, 1977.

[8] R. F. Domagal and D. J. McPherson. System Zirconium-Oxygen. *Trans. AIME*, 200:238–246, 1954.

[9] A. D. McQuillan. Interaction of O and H in Ti. In Jaffee R. I. and Burte H. M., editors, *Proc. 2nd. Int. Conf. Titanium Sci. Technol.*, pages 915–922, 1972.

[10] E. Gebhardt, H. D. Seghezzi, and W. Durrschenabel. Research on the System Zirconium-Oxygen. *J. Nucl. Mater.*, 4:255–268, 1961.

[11] T. Tsuji. Thermochemistry of IVA transition metal-oxygen solid solutions. *J. Nucl. Mater.*, 247:63–71, 1997.

[12] M. Hirabayashi, S. Yamaguci, H. Asano, and K. Hiraga. *Order-Disorder Transformations of Interstitial Solutes in Transition Metals of IV and V Groups*, pages 266–302. Berlin, 1974.

[13] E. G. Rauh and P. Garg. The ZrO_{2-x} (cubic)- ZrO_{2-x} (cubic+tetragonal) Phase Boundary. *J. Am. Ceram. Soc.*, 63:239–240, 1980.

[14] R. J. Ackerman, S. P. Garg, and E. G. Rauh. The Lower Phase Boundary of ZrO_{2-x}. *J. Am. Ceram. Soc.*, 61:275–276, 1978.

[15] R. J. Ackerman, E. G. Rauh, and C. A. Alexander. The Thermodynamic Properties of $ZrO_2(g)$. *High Temp. Sci.*, 7:304–316, 1975.

[16] G. Boureau and P. Gerdanian. High Temperature Thermodynamics of Solutions of Oxygen in Zirconium and Hafnium. *J. Phys. Chem. Solids*, 45:141–145, 1984.

[17] G. Boureau and P. Gerdanian. Use of a Tian-Calvet microcalorimeter at 1300°c direct measurement of $h^M_{O_2}$ in the metal-oxygen systems. *Can. Metall. Q.*, 13:339–343, 1974.

[18] K. L. Komarek and M. Silver. Thermodynamic Properties of Zirconium-Oxygen, Titanium-Oxygen and Hafnium-Oxygen Alloys. In *Thermodynamics of Nuclear Materials*, pages 749–774, Vienna, Austria, 1962. International Atomic Energy Agency.

[19] R. J. Ackerman, S. P. Garg, and E. G. Rauh. The Thermodynamic Properties of Substoichiometric Zirconium Dioxide at the Lower Phase Boundary. *High. Temp. Sci.*, 11:199–210, 1979.

[20] E. G. Rauh and S. P. Garg. The Congruently Vaporizing Compositions and Thermodynamic Properties of the Cubic Phase of Substoichiometric Zirconium Dioxide. *High Temp. Sci.*, 141:121–134, 1981.

[21] W. Wang and D. R. Olander. Thermochemistry of the U-O and Zr-O Systems. *J. Am. Ceram. Soc.*, 76:1242–1248, 1993.

[22] O. Kubaschewski and W. A. Dench. The Dissociation Pressures in the Zirconium-Oxygen System at 100°C. *J. Inst. Met.*, 4:440, 1956.

[23] M. Hillert, B. Jansson, B. Sundman, and Ågren. A Two-Sublattice Model for Molten Solutions With Different Tendency for Ionization. *Metall. Mater. Trans. A*, 16A:261, 1985.

[24] P. Waldner and G. Eriksson. Thermodynamic Modelling of the System Titanium-Oxygen. *CALPHAD*, 23:189–218, 1999.

[25] B. Sundman and J. Agren. A Regular Solution Model for Phases with Several Components and Sublattices, Suitable for Computer Calculations. *J. Phys. Chem. Solids*, 42:297–301, 1981.

[26] R. W. Vest, N. M. Tallan, and W. C. Tripp. Electrical Properties and Defect Structure of Zirconia: I, Monoclinic Phase. *J. Am. Ceram. Soc.*, 47:635–640, 1964.

[27] R. W. Vest and N. M. Tallan. Electrical Properties and Defect Structure of Zirconia: II, Tetragonal Phase and Inversion. *J. Am. Ceram. Soc.*, 48:472–475, 1965.

[28] M. Hillert and B. Jansson. Thermodynamic Model for Non-stoichiometric Ionic Phases. Application to CeO_{2-x}. *J. Am. Ceram. Soc.*, 69:732–734, 1986.

[29] S. C. Carniglia, S. D. Brown, and T. F. Schroeder. Phase Equilbria and Physical Properties of Oxygen-Defficient Zirconia and Thoria. *J. Am. Ceram. Soc.*, 54:13–17, 1970.

[30] O. Kubaschewski, C. B. Alcock, and P. J. Spencer. *Materials Thermochemistry*. Pergamon Press, Oxford, sixth edition, 1993.

A Model Parameters

Note:

- The Gibbs free energies for the species of the Gas phase were obtained from the SGTE Pure Substances Database.
- The Gibbs energies for the reference states for Zr (HCP) and for O ($\frac{1}{2}O_2(g)$) were obtained from the SGTE Solutions Database.
- The Gibbs energies of formation for the stoichiometric ZrO_2 phases were obtained from the JANAF Thermochemical Tables.

Model Parameters for Ionic Liquid $(Zr^{+4})_{4-2y_{O^{-2}}}\ (O^{-2}, Va^{-4})_4$					
$^0G_{Zr_aO_b} - aH_{Zr(HCP),298} - bH_{\frac{1}{2}O_2,298} = {}^0G_{f,Zr_aO_b} + aG^{ref}_{Zr,HCP} + bG^{ref}_{O,\frac{1}{2}O_2}$					
Parameter	$G = A + BT + CT^D; J/mol$				
	A $\times 10^5$	B $\times 10^2$	C	D	T_{min},T_{max}, K
$^0G_{f,(Zr^{+4})_2(O^{-2})_4,L}$	-19.95774	3.024	-9.548×10^{-3}	2	298–6000
$^0G_{f,(Zr^{+4})(Va^{-4})}$	0.181477	-.09080812	1.6275×10^{-22}	7	298–2128
	0.178047	-0.089116	1.3429×10^{31}	-9	2128–6000
$^0L_{(Zr^{+4}:O^{-2},Va^{-4})}(T)$	1.36748	-.6701	0.0	0.0	298–6000
$^1L_{(Zr^{+4}:O^{-2},Va^{-4})}(T)$	0.39995	0.0	0.0	0.0	298–6000

Model Parameters for the BCC Phase $(Zr)_1\,(O,Va)_3$							
$^0G_{Zr_aO_b} - aH_{Zr(HCP),298} - bH_{\frac{1}{2}O_2,298} = {}^0G_{f,Zr_aO_b} + aG^{ref}_{Zr,HCP} + bG^{ref}_{O,\frac{1}{2}O_2}$							
Parameter	$G = A + BT + CT\ln(T) + DT^2 + ET^3 + F/T + GT^H\ J/mol$						T_{min}, T_{max}
$^0G_{(Zr)_1(Va)_3}$	A $\times 10^4$	B $\times 10^2$	C $\times 10^1$	D $\times 10^{-4}$	E $\times 10^{-8}$	F	K
	-0.05255	1.2495	-2.5607	-3.4	-0.9729	25233	298–2128
	G $\times 10^{-11}$	H					
	-7.6143	4					
	A $\times 10^4$	B $\times 10^2$	C $\times 10^1$	G $\times 10^{32}$	H		2128–6000
	-3.075	2.6428	-4.2144	1.2760	-9		
$^0G_{f,(Zr)_1(O)_3}$	A $\times 10^4$	B $\times 10^2$					298–6000
	-40.501	0.0					
$^0L_{(Zr:O,Va)}(T)$	-123.763	2.7601					298–6000

Model Parameters for the HCP Phase $(Zr)_1\,(O,Va)_{0.5}$							
$^0G_{Zr_aO_b} - aH_{Zr(HCP),298} - bH_{\frac{1}{2}O_2,298} = {}^0G_{f,Zr_aO_b} + aG^{ref}_{Zr,HCP} + bG^{ref}_{O,\frac{1}{2}O_2}$							
Parameter	$G, L = A + BT + CT\ln(T) + DT^2 + ET^3 + F/T\ J/mol$						T_{min},T_{max}
	A $\times 10^4$	B $\times 10^2$	C $\times 10^1$	D $\times 10^{-4}$	E $\times 10^{-8}$	F $\times 10^4$	K
$^0G_{(Zr)_1(Va)_{0.5}}$	-0.7827	1.2565	-2.4162	-4.378	0.0	3.4971	130–2128
	-2.6085	2.62724	-4.214	0.0	0.0	0.0	2128–6000
$^0G_{f,(Zr)_1(O)_{0.5}}$	-28.6672	0.4399	0.0	0.0	0.0	0.0	298–6000
$^0L_{(Zr:O,Va)}(T)$	-4.0056	0.1901	0.0	0.0	0.0	0.0	298–6000
$^1L_{(Zr:O,Va)}(T)$	-0.9995	0.0	0.0	0.0	0.0	0.0	298–6000

Model Parameters for Stoichiometric Phases Zr_cO			
$^0G_{Zr_aO_b} - aH_{Zr(HCP),298} - bH_{\frac{1}{2}O_2,298} = {}^0G_{f,Zr_aO_b} + aG^{ref}_{Zr,HCP} + bG^{ref}_{O,\frac{1}{2}O_2}$			
Parameter	$^0G_{f,Zr_cO} = A + BT;\ J/mol$		
	A $\times 10^5$	B $\times 10^2$	T_{min},T_{max}, K
$^0G_{f,Zr_6O}$	-6.500	1.450	298–6000
$^0G_{f,Zr_3O}$	-6.050	0.970	298–6000
$^0G_{f,Zr_2O}$	-5.945	1.101	298–6000

Model Parameters for $\alpha\ ZrO_{2-x}\ (Zr^{+4})_1\ (O^{-2}, Va^{-2})_2$				
$^0G_{Zr_aO_b} - aH_{Zr(HCP),298} - bH_{\frac{1}{2}O_2,298} = {}^0G_{f,Zr_aO_b} + aG^{ref}_{Zr,HCP} + bG^{ref}_{O,\frac{1}{2}O_2}$				
Parameter	$G = A + BT + CT^2;\ J/mol$			
	A $\times 10^5$	B $\times 10^2$	C $\times 10^{-3}$	T_{min},T_{max}, K
$^0G_{f,(Zr^{+4})_1(O^{-2})_2,\alpha\ ZrO_{2-x}}$	-10.96900	1.9393	-4.774	298–6000
$^0G_{f,(Zr^{+4})_1(Va^{-2})_2,\alpha\ ZrO_{2-x}}$	2.00	0.0	0.0	298–6000
$^0L_{(Zr:O,Va)}(T)$	0.0	0.0	0.0	298–6000

Model Parameters for $\beta\ ZrO_{2-x}\ (Zr^{+4})_1\ (O^{-2}, Va^{-2})_2$				
$^0G_{Zr_aO_b} - aH_{Zr(HCP),298} - bH_{\frac{1}{2}O_2,298} = {}^0G_{f,Zr_aO_b} + aG^{ref}_{Zr,HCP} + bG^{ref}_{O,\frac{1}{2}O_2}$				
Parameter	$G = A + BT + CT^2;\ J/mol$			
	A $\times 10^5$	B $\times 10^2$	C $\times 10^{-3}$	T_{min},T_{max}, K
$^0G_{f,(Zr^{+4})_1(O^{-2})_2,\beta\ ZrO_{2-x}}$	-11.02841	1.8991	-4.774	298–6000
$^0G_{f,(Zr^{+4})_1(Va^{-2})_2,\beta\ ZrO_{2-x}}$	2.00	0.0	0.0	298–6000
$^0L_{(Zr:O,Va)}(T)$	-1.3021	0.3503	0.0	298–6000
$^1L_{(Zr:O,Va)}(T)$	-0.1999	0.0	0.0	298–6000

Model Parameters for $\gamma\ ZrO_{2-x}\ (Zr^{+4})_1\ (O^{-2}, Va^{-2})_2$				
$^0G_{Zr_aO_b} - aH_{Zr(HCP),298} - bH_{\frac{1}{2}O_2,298} = {}^0G_{f,Zr_aO_b} + aG^{ref}_{Zr,HCP} + bG^{ref}_{O,\frac{1}{2}O_2}$				
Parameter	$G = A + BT + CT^2; J/mol$			
	A $\times 10^5$	B $\times 10^2$	C $\times 10^{-3}$	T_{min},T_{max}, K
$^0G_{f,(Zr^{+4})_1(O^{-2})_2,\gamma\ ZrO_{2-x}}$	-11.08886	1.8762	-4.774	298–6000
$^0G_{f,(Zr^{+4})_1(Va^{-2})_2,\gamma\ ZrO_{2-x}}$	2.00	0.0	0.0	298–6000
$^0L_{(Zr:O,Va)}(T)$	-2.3585	0.23	0.0	298–6000
$^1L_{(Zr:O,Va)}(T)$	-1.0544	0.0	0.0	298–6000
$^2L_{(Zr:O,Va)}(T)$	1.8491	0.0	0.0	298–6000